ЖЭТФ, 2011, том 139, вып. 6, стр. 1119–1126

TEMPERATURE-INDUCED TRANSFORMATIONS IN HYDROGENATED AND FLUORINATED SINGLE-WALL CARBON NANOTUBES STUDIED BY RAMAN SCATTERING

K. P. Meletov [a*], ***A. A. Maksimov*** [a], ***I. I. Tartakovskii*** [a], ***J. Arvanitidis*** [b,c], ***D. Christofilos*** [b], ***G. A. Kourouklis*** [b]

[a] *Institute of Solid State Physics, Russian Academy of Sciences 142432, Chernogolovka, Moscow Region, Russia*

[b] *Physics Division, School of Technology, Aristotle University of Thessaloniki 54124, Thessaloniki, Greece*

[c] *Department of Applied Sciences, Technological Educational Institute of Thessaloniki 57400, Sindos, Greece*

Received October 22, 2010

Raman spectra of hydrogenated and fluorinated single-wall carbon nanotubes (SWCNTs) are measured at ambient temperature before and after heat treatment. The spectra of the as-prepared hydrogenated SWCNTs show a giant structureless band in the visible region that screens the Raman peaks related to the carbon atom vibrations. The onset of this strong band follows the excitation laser line, which is typical for hot luminescence. The intensity of the luminescence background decreases exponentially with the annealing time, while the dependence of the luminescence decay time constant on the annealing temperature is of the Arrhenius type with the activation energy $E_a = 465 \pm 44$ meV. The luminescence background in the Raman spectra of the fluorinated SWCNTs is comparable with the Raman peak intensity and decreases exponentially with the annealing time. The dependence of the decay time constant on the temperature is again of the Arrhenius type with the activation energy $E_a = 90 \pm 8$ meV. The appearance of hot luminescence is related to the upshift of the fundamental energy gap in functionalized SWCNTs and the structural disorder induced by random binding of hydrogen or fluorine atoms. The luminescence background disappears upon annealing in a vacuum or in air after removal of hydrogen (fluorine), while the annealed samples still demonstrate large structural disorder.

1. INTRODUCTION

Single-wall carbon nanotubes (SWCNTs) are candidates for hydrogen storage because molecular hydrogen can potentially fill the interior of the tubules or the space between them within the bundles [1]. A good storage medium must have a potential to adsorb a high density of hydrogen, and carbon nanotubes are being widely investigated for this reason [2–5]. Alternatively, hydrogen atoms can form covalent bonds with carbon atoms in an SWCNT due to the existence of a large number of unsaturated double C=C bonds as in the case of fullerene C_{60} [6]. For example, hydrogenation of C_{60} fullerene results in the formation of stable $C_{60}H_{18}$ and $C_{60}H_{36}$ compounds, where hydrogen and carbon atoms are covalently bonded [7, 8]. Reported efficiencies of the hydrogen uptake in the hydrogenated SWCNTs (SWCNT-H) vary between 4 and 8 wt. % of both molecular and covalently bonded hydrogen. The hydrogenation of SWCNTs reported by a number of research groups was performed at ambient conditions, as well as at an increased hydrogen pressure and liquid-nitrogen temperature [2, 3]. The high-pressure/high-temperature hydrogenation of SWCNTs was predicted theoretically to be very effective [4] and a recent work at the hydrogen pressure 9 GPa and the temperature 450 °C has resulted in stable SWCNT-H at ambient conditions, containing near 6.5 wt. % of hydrogen [5]. The IR absorption spectra of SWCNT-H show C–H vibration bands related to covalently bonded hyd-

*E-mail: mele@issp.ac.ru

rogen that partially disappear after hydrogen removal to the residual content of 3 wt. % upon annealing at increased temperatures [5]. Raman spectroscopy has been successfully used in the study of the C–H covalent bonds in fullerene hydrides [8], as well as in the study of the molecular hydrogen physisorption on the ropes of SWCNTs [9]. In carbon-related materials, the covalently bonded hydrogen exhibits intense and relatively broad Raman peaks, associated with the C–H stretching vibrations that shift to lower energies when hydrogen is substituted by deuterium. In contrast, the adsorbed molecular hydrogen exhibits narrow peaks, which are associated with the H–H stretching vibration mode. In the fluorinated SWCNTs (SWCNT-F), the covalent bonding between carbon and fluorine atoms also results in the appearance of C–F stretching vibration modes [10, 11].

A comparative Raman study of the as-prepared and annealed SWCNT-H and SWCNT-F samples would give important information related to the covalent bonding of hydrogen and fluorine atoms as well as to adsorbed molecular hydrogen. In view of this, we have measured the Raman spectra of the as-prepared SWCNT-H and SWCNT-F samples at ambient conditions and found that SWCNT-H show intense structureless luminescence background that screens the Raman peaks related to the carbon atom vibrations. The onset of the background follows the excitation laser line, which is typical of hot luminescence. The luminescence background gradually decreases upon annealing of the SWCNT-H in a vacuum or in air. The Raman spectra of the annealed hydrogenated (SWCNT-H) and deuterated (SWCNT-D) samples have been compared to that of molecular hydrogen to clarify the contributions of molecular and covalently bonded hydrogen. In addition, *in-situ* Raman spectra of SWCNT-H have been recorded upon annealing in air in order to study the process of the hydrogen removal due to its oxidation.

The luminescence background of the SWCNT-H decreases exponentially with the annealing time and the dependence of the decay time constant on the annealing temperature is of the Arrhenius type, with the activation energy $E_a = 465 \pm 44$ meV. The Raman spectra of the annealed samples demonstrate large structural disorder, most likely related to the defects induced upon both high-pressure/high-temperature hydrogenation and hydrogen removal at the increased temperature. No traces of molecular hydrogen associated with the H–H stretching vibration of hydrogen atoms were found in the Raman spectra of the as-prepared and annealed SWCNT-H. The SWCNT-F has initially a lower luminescence background, which is comparable with the Raman peak intensities. The luminescence intensity decreases upon annealing, while its time dependence can be fitted by two exponentials associated with a fast and a slow decay time constants. The dependence of the slow decay time constant on the annealing temperature is of the Arrhenius type with activation energy $E_a = 90 \pm 8$ meV.

2. EXPERIMENTAL DETAILS

The starting SWCNT was synthesized by the arc discharge evaporation method in helium atmosphere at the pressure 0.86 bar using a metallic Ni/Y catalyst. A purification method based on the multistep oxidation in air followed by multistep reflux in HCl resulted in an approximately 90 wt. % content of SWCNT. The average SWCNT diameter was 1.5 nm (1.4–1.6 nm), as it follows from the preparation method and the transmission electron microscopy characterization. No surfactants were used during the purification procedure. The final material was a black fluffy powder that consisted of large (about 100 μm) nanotube mats. The main impurities were graphite nanoparticles of the order of 2–4 μm in size, and the total content of metal impurities was near 1.3 %. The final product was annealed in a vacuum at 600 °C for 5 h.

The SWCNTs were hydrogenated at a high hydrogen pressure and high temperature. A mass of 60 mg from the SWCNT material was placed in a high-pressure chamber and saturated with hydrogen obtained by thermal decomposition of AlH_3. The sample was held under the hydrogen pressure 5 GPa at 500 °C for 10 h. The obtained SWCNT-H samples, containing up to 5.5 wt. % of hydrogen, were kept in a cold-welded aluminum container. The samples are stable at ambient conditions as the major hydrogen content is released at $T \geq 500$ °C in a vacuum, in agreement with an earlier study [5]. The high-pressure/high-temperature hydrogenation procedure was the same as the one used for hydrogenation of the C_{60} fullerene and described elsewhere [12].

The purified SWCNT samples synthesized as described above were fluorinated in a custom-built fluorination apparatus for 5 h at 180 °C and at the fluorine pressure 0.8 bar. The fluorinated material was sonicated in ethanol for 10 min and then the dispersed material, separated from sediment, was filtered through a 0.2-μm filter and dried. The obtained SWCNT-F samples contained approximately 25.4 wt. % of fluorine according to the data of the ionic elemental analysis.

Raman spectra from small SWCNT-H and SWCNT-F pieces with typical dimensions of 100 μm were recorded in the backscattering geometry using two different micro-Raman setups (DILOR XY), both comprising a triple monochromator and a CCD detector system, cooled at the liquid-nitrogen temperature. The 488-nm and 514.5-nm lines of an Ar^+ laser, and the 647.1-nm line of a Kr^+ laser, were used for excitation, while the beam intensity on the sample was varied in the range 0.04–0.5 mW. The laser line was focused on the sample by means of a long working distance 50× objective with the spatial resolution approximately 1.5 μm. The high-temperature Raman measurements were performed by the use of a home-made high-temperature cell with a temperature controller that can maintain temperatures up to 750 K with the accuracy of ±2 K.

3. RESULTS AND DISCUSSION

Raman spectra of the initially purified and hydrogenated SWCNTs are shown in Fig. 1. The spectrum in Fig. 1*a* corresponds to the purified SWCNT; its narrow peaks and the weak D band at 1350 cm^{-1} are typical of SWCNTs with a high structural order. The appearance and the dispersive behavior of the D band in graphite-related materials are associated with a structural disorder, and a double-resonance process was used for their interpretation [13]. The intense G band at a higher energy corresponds to the C–C stretching vibrations in tangential and axial directions of the SWCNT, which splits to G^- and G^+ bands located at 1567 cm^{-1} and 1592 cm^{-1}, respectively. The shape of the G^- band is sensitive to the electronic SWCNT properties (strongly related to chirality), the Lorentzian lineshape is characteristic of semiconducting SWCNTs, whereas a Breit–Wigner–Fano lineshape is typical of metallic SWCNTs [14]. In the spectrum shown in Fig. 1*a*, the Lorentzian lineshape of the G^- band indicates that the SWCNTs probed by the 514.5 nm excitation are mainly semiconducting. The low-frequency Raman band related to the radial breathing modes of the tubules is composed of a prominent peak located at 166 cm^{-1} and a high-energy shoulder near 178 cm^{-1}. The frequency ω_R of these modes is inversely proportional to the tube diameter D_t, and its value is up-shifted owing to the interaction of tubules within the bundle [14]. One of the empirical relations between D_t and ω_R, applicable for bundled SWCNTs, is [14]

$$D_t\ [\text{nm}] = \frac{234\ \text{nm}\cdot\text{cm}^{-1}}{\omega_R\ [\text{cm}^{-1}] - 12\ \text{cm}^{-1}}. \qquad (1)$$

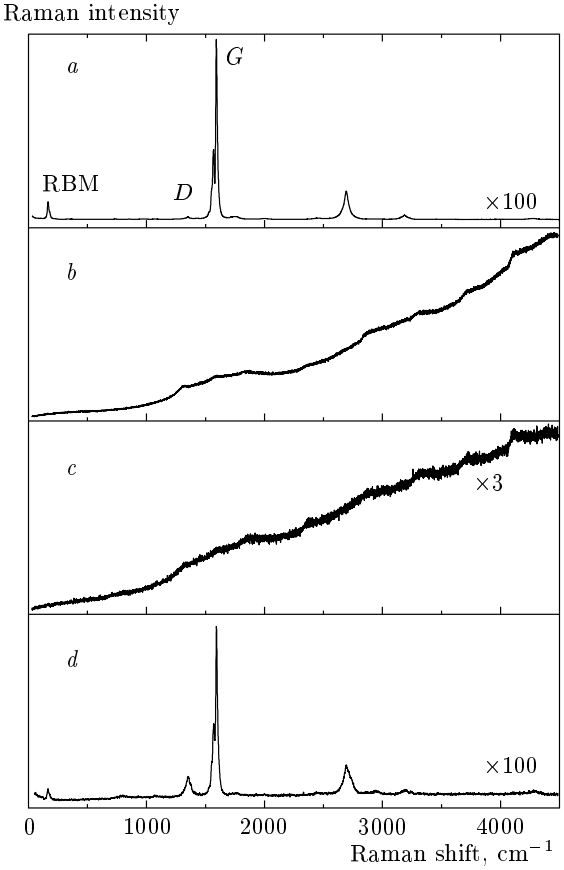

Fig. 1. Raman spectra of (*a*) purified pristine SWCNT and (*b*)–(*d*) SWCNT-H after annealing in a vacuum at $T \approx 200\,^\circ$C for $t = 180$ min (*b*), $T \approx 350\,^\circ$C for 180 min (*c*), and $T \approx 550\,^\circ$C for 60 min (*d*); RMB is a radial breathing mode

According to Eq. (1), the main radial-breating mode peak at 166 cm^{-1} corresponds to the SWCNT with the diameter about 1.52 nm, whereas the shoulder at 178 cm^{-1} is related to the SWCNT with the diameter about 1.41 nm. These tube diameters are in good agreement with those estimated by the transmission electron microscopy (TEM) observations.

The diffuse and structureless spectrum in Fig. 1*b* refers to SWCNT-H. Its intensity is about a hundred times stronger than that of the purified SWCNTs due to the luminescence background that screens the Raman peaks related to carbon atom vibrations. The high intensity and the frequency dependence of this feature are typical characteristics of hot luminescence. This is further supported by the fact that the luminescence background intensity and frequency dependence do not change if we alternatively use the 647.1-nm laser line for excitation (not shown). We note that the spec-

trum was recorded after annealing of the as-prepared SWCNT-H samples in a vacuum at 200 °C for 3 h, whereas before annealing, the background is even more intense. Its intensity differs somehow between samples taken from the same batch and decreases under intense laser irradiation. Therefore, the Raman measurements were performed at very low laser intensities on sample (0.04–0.5 mW). The background intensity further decreases after the subsequent vacuum annealing at 350 °C for 3 h (Fig. 1*c*), but the most prominent changes occur after an additional vacuum annealing at 550 °C for 1 h (Fig. 1*d*). The spectrum in Fig. 1*d* has the lowest luminescence background and comprises the basic Raman features of the as-prepared SWCNT, i. e., the radial breahing mode, the D band and the split G band as well as second-order Raman peaks above 2000 cm^{-1}. The increased intensity of the D band and the peak broadening are indicative of a higher structural disorder of the annealed SWCNT-H compared to that in purified SWCNTs.

The second-order Raman peaks in the spectra of the purified SWCNTs, related to the double-resonance one- and two-phonon processes giving rise to overtones and combination modes, become more intense in the spectrum of the annealed SWCNT-H sample [13, 15, 16]. These peaks include the $2D$ mode (2692 cm^{-1}), the $D + G^-$ and $D + G^+$ combination modes (2917–2942 cm^{-1}), the $2G^-$ mode (3133 cm^{-1}), the $G^- + G^+$ combination mode (3160 cm^{-1}), and the $2G^+$ mode (3186 cm^{-1}). The Raman modes associated with the C–H stretching vibrations of the covalently bonded hydrogen are also expected in the frequency region 2800–3200 cm^{-1}. These modes are downshifted upon deuterium substitution of hydrogen.

To verify the origin of the observed peaks in the frequency region of interest, we have measured the Raman spectra of the SWCNT-D samples prepared by the same method and conditions as the SWCNT-H. These samples have been characterized by mass spectroscopy, and have been found to contain approximately 10.5 wt. % deuterium [17], indicating the atomic concentration of the light element similar to that in SWCNT-H. The Raman spectra of the as-prepared SWCNT-D also demonstrate a giant luminescence background that decreases under vacuum annealing. Raman spectra of SWCNT-H and SWCNT-D both annealed in a vacuum at 550 °C for 1 h are illustrated in Fig. 2. The two spectra are nearly identical and their comparison to that of the purified SWCNT indicates the increased structural disorder of SWCNT-H and SWCNT-D. No isotopic shift is observed, suggesting that the observed peaks are not related to covalently

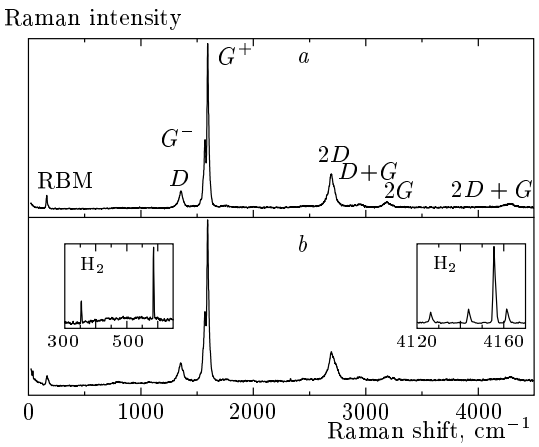

Fig. 2. Raman spectra of (a) SWCNT-H and (b) SWCNT-D samples after annealing in a vacuum at $T \approx 550$ °C for 60 min. Inserts: Raman spectra at two different spectral regions of molecular hydrogen at 5 bar

bonded hydrogen. Consequently, the SWCNT-H and SWCNT-D samples annealed at 550 °C for 1 h do not contain any significant amount of covalently bonded hydrogen, in consistency with the mass-spectroscopy data [17]. The weak peaks in the Raman spectrum of the annealed SWCNT-H at 4259 cm^{-1} and 4284 cm^{-1} lie closely to the Raman frequencies of molecular hydrogen (4130–4160 cm^{-1}). In search for adsorbed molecular hydrogen, we have measured the Raman spectrum of pure molecular hydrogen at $P \approx 5$ bar, obtained by thermal decomposition of AlH_3 in a quartz vessel. The Raman spectrum of molecular hydrogen shown in the inserts in Fig. 2*b* consists of two very sharp peaks at 353 and 587 cm^{-1}, related to librations of the H_2 molecule, and six sharp peaks at 4126, 4143, 4155, and 4161 cm^{-1}, related to the H–H roto-vibrations. Obviously, the Raman spectrum of the annealed SWCNT-H does not contain any sharp peaks in these frequency regions, but rather the weak and broad Raman features at 4259 and 4284 cm^{-1} mentioned above, which remain unaffected upon hydrogen substitution by deuterium. Therefore, these peaks should be attributed to the second-order $2D + G^-$ and $2D + G^+$ combination modes. Finally, the Raman spectrum of SWCNT-H sample in Fig. 2*a* does not contain any peaks in the range 300–500 cm^{-1}, where the librations of the hydrogen molecule are observed.

The luminescence background decreases faster and at a lower temperature when the annealing occurs in air rather than in a vacuum, due to the oxidation and the more efficient removal of covalently bonded hydro-

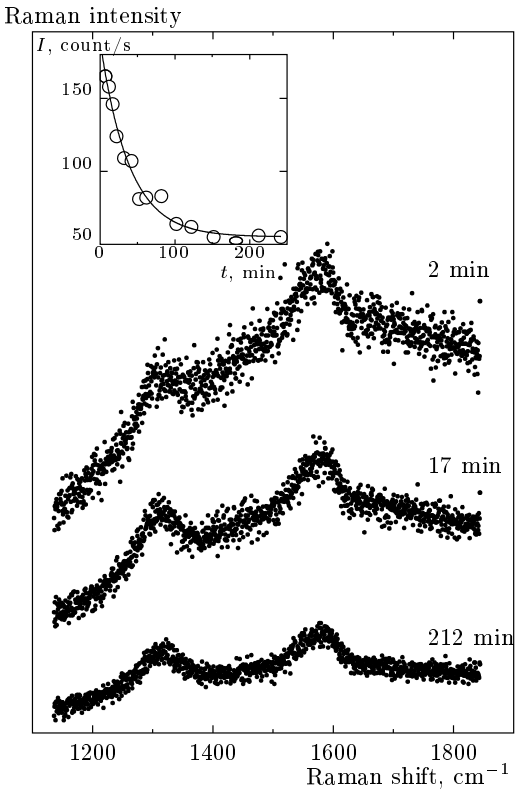

Fig. 3. Raman spectra in the frequency range of the D and the G bands for the SWCNT-H after 2, 17, and 212 min annealing in air at 160 °C. Insert: the dependence of the luminescence background intensity on the annealing time

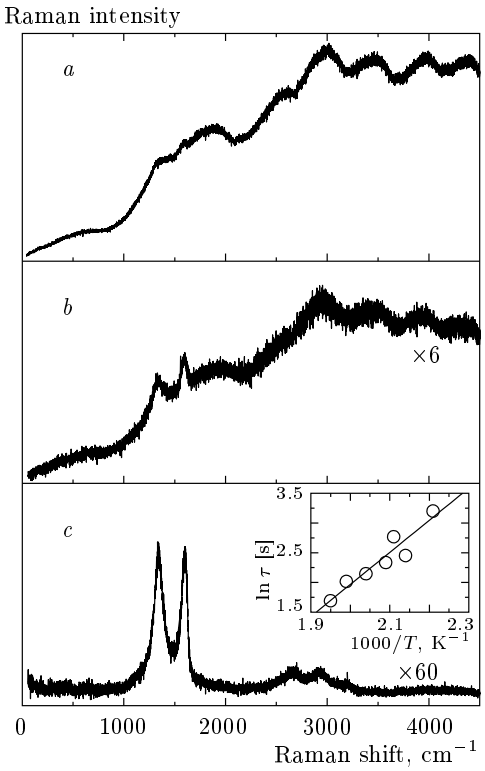

Fig. 4. Raman spectra of (a) as-prepared SWCNT-H, (b) SWCNT-H after annealing in air at $T \approx 180$ °C for 20 min, and (c) after additional annealing in air at $T \approx 230$ °C for 20 min. Insert: Arrhenius plot of the luminescence decay time constant ($E_a = 465 \pm 44$ meV)

gen. Figure 3 shows the *in-situ* Raman spectra of the SWCNT-H sample measured in the frequency range of D and G bands upon annealing of samples in air at 160 °C. To avoid the additional heating of samples induced by the laser beam, its intensity was kept as low as 0.04 mW. The spectra measured at a fixed site of the sample during the long annealing time show a gradual decrease in the luminescence background. The dependence of the background intensity on the annealing time is exponential (see the insert in Fig. 3), while the decay time constant decreases with an increase in the annealing temperature.

Figure 4 illustrates the room-temperature Raman spectra of SWCNT-H sample recorded *in-situ* at a fixed site of the sample before and after a 20-min annealing in air at 180 °C. The Raman spectrum of the sample after an additional 20-min annealing at 230 °C is also included (Fig. 4c). These spectra clearly show that the annealing in air is more efficient than in a vacuum. The intense D band in the spectra of SWCNT-H samples after annealing in air indicates their enhanced structural disorder compared to the samples annealed in a vacuum. The insert in Fig. 4 shows the dependence of the decay time constant on the annealing temperature obtained from the *in-situ* measurements of the luminescence intensity at various annealing temperatures. We can estimate the activation energy of the hydrogen removal by taking into account that the decay time constant versus the annealing temperature T is described by an Arrhenius-type equation

$$\tau(T) = A \exp(E_a/k_B T), \qquad (2)$$

where k_B is the Boltzmann constant and τ is the time constant of the luminescence decay. The constant A is related to the characteristic phonon frequency and is measured in time units. The activation energy calculated from our data is $E_a = 465 \pm 44$ meV. This value refers not to the C–H bond energy but to the activation of the reaction, which results in the removal of bonded hydrogen due to its oxidation.

The *in-situ* Raman spectra of the as-prepared and

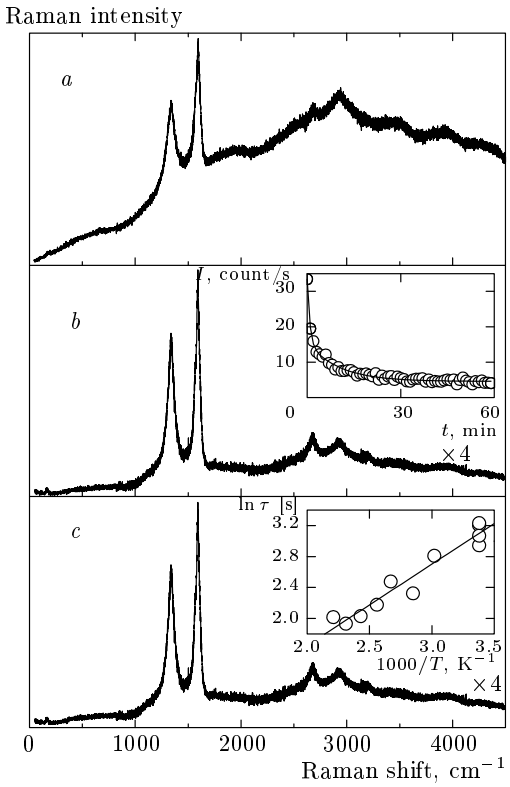

Fig. 5. Raman spectra of (a) as-prepared SWCNT-F, (b) SWCNT-F after annealing in air at $T \approx 200\,^{\circ}$C for 60 min, and (c) after additional annealing in air at $T \approx 300\,^{\circ}$C for 50 min. Inserts: (b) the dependence of the luminescence background intensity on the annealing time and (c) Arrhenius plot of the luminescence decay time constant ($E_a = 90 \pm 8$ meV)

annealed in air SWCNT-F sample are shown in Fig. 5. Figure 5a shows the Raman spectrum of the as-prepared SWCNT-F characterized by the D and G bands superposed on a structureless luminescence background. A similar luminescence background was observed earlier in the Raman spectra of SWCNT-F fluorinated at 250 °C [18]. The luminescence background decreases with an increase in the fluorination temperature and almost disappears in the samples fluorinated at 400 °C [19]. The defluorination of SWCNT-F, performed by annealing in air [20] or by reaction with anhydrous hydrazine [19], leads in both cases to the disappearance of the luminescence background associated with the removal of bonded fluorine. In our case, the luminescence background rapidly decreases under the annealing of SWCNT-F in air, resulting in the domination of the Raman D and G bands in the spectrum of the sample annealed at 200 °C for 60 min (Fig. 5b). Further annealing of this sample at 300 °C for 50 min does not change the Raman spectrum significantly, which demonstrates a relatively low luminescence background and typical features of highly disordered SWCNTs (Fig. 5c). Despite the high structural disorder associated with the presence of a strong D band and a broad G band, a weak radial-breathing-mode peak also appears in the spectrum.

The annealing process in SWCNT-F is faster and occurs at lower temperatures compared to that for SWCNT-H. The dependence of the luminescence background intensity on the annealing time can be reliably described by two exponential terms of the shorter and the longer decay time constants (Fig. 5b, insert). The fast-decay time constant is independent of the annealing temperature, while the slow-decay time constant is comparable with that of the SWCNT-H and decreases as the annealing temperature increases. The independence of the fast-decay time constant on the treatment temperature may be related to some photostimulated process that also results in fluorine removal. In any case, our results are insufficient to make a conclusion, and this effect needs further study. The insert in Fig. 5c shows the dependence of the slow-decay time constant on the annealing temperature, obtained from a series of *in-situ* measurements of the luminescence intensity reduction at various annealing temperatures. This dependence can be fitted by an Arrhenius-type equation, yielding the activation energy $E_a = 90 \pm 8$ meV for the removal of the bonded fluorine. As in the case of SWCNT-H samples, this value refers not to the C–F bond energy but to the activation of the reaction with atmospheric gases, resulting in the removal of bonded fluorine.

In contrast to hydrogenated carbon materials, the C–F stretching vibration, resulting in a rather strong peak in the IR absorption spectra at 1260 cm^{-1}, is very weak in the Raman spectra of SWCNT-F due to the small polarization of the C–F bond [18, 19]. Hence, the main effects of SWCNT fluorination in the Raman spectrum are the appearance of the background luminescence, the broadening of the peaks related to carbon atom vibrations, and the intensity enhancement of the D band. These effects are indications of an increased structural disorder in SWCNT-F. In addition, it was shown that the fluorination of open-end SWCNTs results in less structural disorder than that of closed-end SWCNTs with the same concentration of fluorine, as follows from the higher intensity of the D band in the Raman spectra [20]. All these data indicate that the random creation of C–F covalent bonds upon nanotube fluorination distorts the translational symmetry and induces structural disorder manifested in the Raman

spectra by an intense D band. On the other hand, the annealing of SWCNT-F induces additional defects related to the removal of fragments comprising carbon atoms bonded to fluorine [19].

It is interesting to compare the Raman data with those obtained from the IR spectra of the as-prepared SWCNT-H, which show distinct C–H stretching vibration peaks [5]. The IR bands demonstrate large isotopic shifts in SWCNT-D due to deuterium substitution of hydrogen. The peak intensity in the IR spectra of SWCNT-H gradually decreases upon vacuum annealing and the peaks eventually disappear at 550 °C following the removal of hydrogen [5].

Contrary to the case of the IR spectra, the main characteristic of the Raman spectrum of SWCNT-H is the giant luminescence background, which masks the Raman peaks, thus preventing the observation of the C–H and H–H stretching vibrations. We note that bundling effects in SWCNTs result in the quenching of light emission, possibly due to the presence of some amount of metallic nanotubes within the bundles, whereas debundling in sonicated solution and separation of the nanotubes leads to the appearance of IR luminescence [21, 22]. The hydrogenation of SWCNTs should result in the upshift of the fundamental gap of semiconducting nanotubes similar to fullerene hydride $C_{60}H_{36}$ [23], as well as to a possible transformation of metallic nanotubes into semiconducting ones. The latter cancels the luminescence quenching in SWCNT bundles and could explain the appearance of the strong luminescence background in the visible range.

At the same time, the structural disorder induced by formation of the C–H and C–F covalent bonds randomly distributed over SWCNTs results in the lifetime reduction of the excited states, and fluorescence is replaced by the observed hot luminescence. The luminescence background disappears upon the annealing of SWCNT-H and SWCNT-F at high temperature in accordance with the removal of bonded hydrogen and fluorine, respectively. Evidently, the absence of the C–H and H–H stretching vibration peaks in the Raman spectra of the annealed SWCNT-H and SWCNT-D is related to the vanishingly small density of covalently bonded atomic hydrogen and adsorbed molecular hydrogen.

4. CONCLUSIONS

Summarizing, the Raman spectra of the fluorinated and hydrogenated SWCNTs show an intense and structureless luminescence background that interferes with or completely screens the peaks related to the carbon atom vibrations. The onset of the background follows the excitation laser line, typical of hot luminescence. The observed hot luminescence may be attributed to the upshift of the energy gaps in functionalized SWCNTs and the structural disorder induced by random binding of hydrogen/fluorine atoms. The luminescence background gradually decreases upon sample annealing in a vacuum or in air. The Raman spectra of the annealed SWCNT-H and SWCNT-D do not show any peaks related to C–H stretching vibrations or peaks related to the H–H vibrations or librations of molecular hydrogen, associated with covalently bonded or adsorbed molecular hydrogen. The luminescence background of the SWCNT-H decreases exponentially with the annealing time and the dependence of the decay time constant on the annealing temperature is of an Arrhenius type, with the activation energy 465 ± 44 meV. The Raman spectra of the annealed samples demonstrate large structural disorder, most likely related to the defects induced both by high-pressure/high-temperature hydrogenation and by hydrogen removal at increased temperature. The fluorinated carbon nanotubes initially have a lower luminescence background, comparable to the Raman peak intensity. The luminescence intensity decreases again upon annealing, and the time dependence of this reduction can be well fitted by two exponentials with fast- and slow-decay time constants. The dependence of the slow-decay time constant on the annealing temperature is also of the Arrhenius type, associated with the activation energy 90 ± 8 meV.

The authors thank A. V. Krestinin and I. O. Bashkin for providing SWCNT samples. One of the authors (K. P. M.) acknowledges the hospitality of the Aristotle University of Thessaloniki, Greece. The support by the RFBR (grant No. 08-02-00890) is acknowledged.

REFERENCES

1. S. J. V. Frankland and D. W. Brenner, Chem. Phys. Lett. **334**, 18 (2001).

2. A. C. Dillon, K. M. Jones, T. A. Bekkedahl et al., Nature **386**, 377 (1997).

3. Y. Ye, C. C. Ahn, C. Witham et al., Appl. Phys. Lett. **74**, 2307 (1999).

4. S.-P. Chan, G. Chen, X. G. Gong, and Z.-F. Liu, Phys. Rev. Lett. **87**, 205502 (2001).

5. I. O. Bashkin, V. E. Antonov, A. V. Bazhenov et al., Pis'ma v Zh. Eksp. Teor. Fiz. **79**, 280 (2004).

6. R. Bini, J. Ebenhoch, M. Fanti et al., Chem. Phys. **23**, 75 (1998).

7. A. I. Kolesnikov, V. E. Antonov, I. O. Bashkin et al., J. Phys.: Condens. Matter **9**, 2831 (1997).

8. K. P. Meletov, S. Assimopoulos, I. Tsilika et al., Chem. Phys. **263**, 379 (2001).

9. K. A. Williams, B. K. Pradhan, P. C. Eklund et al., Phys. Rev. Lett. **88**, 165502 (2002).

10. E. T. Mickelson, C. B. Huffman, A. G. Rinzler et al., Chem. Phys. Lett. **296**, 188 (1998).

11. S. Kawasaki, K. Komatsu, F. Okino et al., Phys. Chem. Chem. Phys. **6**, 1769 (2004).

12. V. E. Antonov, I. O. Bashkin, S. S. Khasanov et al., J. Alloy Comp. **330**, 365 (2002).

13. C. Thomsen and S. Reich, Phys. Rev. Lett. **85**, 5214 (2000).

14. U. D. Venkateswaran, Phys. Stat. Sol. (b) **241**, 3345 (2004).

15. R. Saito, A. Jorio, A. G. Souza Filho et al., Phys. Rev. Lett. **88**, 027401 (2002).

16. V. W. Brar, Ge. G. Samsonidze, M. S. Dresselhaus et al., Phys. Rev. B **66**, 155418 (2002).

17. Yu. M. Shulga, I. O. Bashkin, A. V. Krestinin et al., Pis'ma v Zh. Eksp. Teor. Fiz. **80**, 884 (2004).

18. P. E. Pehrsson, W. Zhao, J. W. Baldwin et al., J. Phys. Chem. **107**, 5690 (2003).

19. E. T. Mickelson, C. B. Huffman, A. G. Rinzler et al., Chem. Phys. Lett. **296**, 188 (1998).

20. S. Kawasaki, K. Komatsu, F. Okino, and H. Kataura, Phys. Chem. Chem. Phys. **6**, 1769 (2004).

21. J. Wu, W. Walukiewicz, W. Shan et al., Phys. Rev. Lett. **93**, 017404 (2004).

22. D. Karaiskaj, C. Engtrakul, T. McDonald et al., Phys. Rev. Lett. **96**, 106805 (2006).

23. K. P. Meletov, S. Assimopoulos, G. A. Kourouklis, and I. O. Bashkin, Fiz. Tverd. Tela **44**, 519 (2002).